Conserved quantities and adaptation to the edge of chaos

Michael Baym* and Alfred W. Hübler†
Santa Fe Institute, 1399 Hyde Park Road, New Mexico 87501, USA
(Received 28 May 2005; revised manuscript received 9 March 2006; published 26 May 2006)

Certain dynamical systems, such as the shift map and the logistic map, have an edge of chaos in their parameter spaces. On one side of this edge, the dynamics are chaotic for many parameter values, on the other side of the edge they are periodic. We find that discrete-time dynamical systems with wavelet filtered feedback from the dynamical variable to the parameters are attracted to a narrow parameter range near the edge of chaos, the periodic boundary regime. We show that the migration from the chaotic regime to the periodic boundary regime can be attributed to a conserved quantity, and find that such adaptation to the edge of chaos is accompanied by a depopulation of the chaotic regime. We use this conserved quantity to determine the location of the periodic boundary regime and show that its size is proportional to the size of the feedback. Further, we compute the dynamics of the probability density for the parameter for a specific example.

DOI: 10.1103/PhysRevE.73.056210 PACS number(s): 05.45.Ac, 05.45.Tp, 05.65.+b

I. INTRODUCTION

The concept "adaptation to the edge of chaos" refers to the idea that many complex adaptive systems, including those found in biology, seem to naturally evolve toward a narrow regime near the boundary between order and chaos [1]. The suppression of chaos is not due to a sophisticated external control [2–9] but induced by some simple self-adjustment of the system. Packard [10] first showed that adaptation to the edge of chaos occurs for a population of cellular automata rules evolving with a genetic algorithm, though the conclusions drawn from this work have come under some dispute [11]. Self-organized critically (SOC) [12] in avalanche and earthquake models is believed to be a related phenomenon. However the connection between SOC and edge of chaos is not completely obvious. This is mainly due to the fact that in the SOC models (e.g., the sand pile) some randomness is involved; therefore there is not a unique way to define the Lyapunov exponent and this can induce some confusion [13–15]. Models of coupled neurons with self-adjusting coupling strength have been found to exhibit robust synchronization and suppression of chaos [16]. The edge of chaos occupies a prominent position because it has been found to be not only the optimal setting for control of a system [17], but also an optimal setting under which a physical system can support primitive functions for computation [18], though once again this claim has been disputed [19]. Zaslavsky and others [20,21] noted that the irregular dynamics near the edge of chaos has unique properties due to very long transients and they call that motion pseudochaos.

Possibly the simplest models for adaptation to the edge of chaos are self-adjusting map dynamics [22]. The numerical findings have been confirmed experimentally [23] with Chua's circuit [24]. However, the theoretical analysis does not predict the location of the narrow parameter regime near the boundary to which the system evolves. Furthermore the distribution function for the limiting parameter values differ from numerical findings. This is believed to be due to the fact that the dynamics of the parameters are approximated by a diffusion process with a large diffusion constant in the chaotic regime. In Melby's system, the feedback from the dynamical variable to the map parameter is computed with a windowed Fourier band filter. This is a rather complicated algorithm whereas wavelet filters [25,26] have a similar effect, but are much simpler in both implementation [27–29] and analysis. Wavelet filters have been successfully used for the compression of experimental data [30–37] as well as images in JPEG format [38]. Finitely supported wavelet filters can be good models for the dynamics of slow variables in naturally occurring processes [39,40], though not all wavelets filters have these properties [41].

In this paper, we study the evolution of self-adjusting maps toward the edge of chaos. Maps can be good models nonlinear and chaotic motion, and are mathematically more tractable than nonlinear differential equations. In contrast to earlier work, we assume that the feedback from the dynamical variable is low-pass wavelet filtered. Wavelet filters can mimic the filter function of damped oscillators which occur in many natural systems. We use discrete wavelet filters that have a finite support and have zero mean. Further we consider the impact of correlations in the parameter dynamics and determine the location of the narrow regime near the edge of chaos to which the dynamics evolve. Finally we determine the dynamics of the probability density of the parameter for a specific example.

II. SELF-ADJUSTING MAP DYNAMICS

We consider a self-adjusting map dynamics with the dynamical variable x_n on the interval [0,1] and a self-adjusting parameter a_n

$$x_{n+1} = f(x_n, a_n),$$

*Current address: Department of Mathematics, MIT, 77 Massachusetts Ave., Cambridge, MA 02139.
†Permanent address: Center for Complex Systems Research, Department of Physics, 1110 W Green Street, University of Illinois at Urbana-Champaign, Illinois 61801; electronic address: a-hubler@uiuc.edu

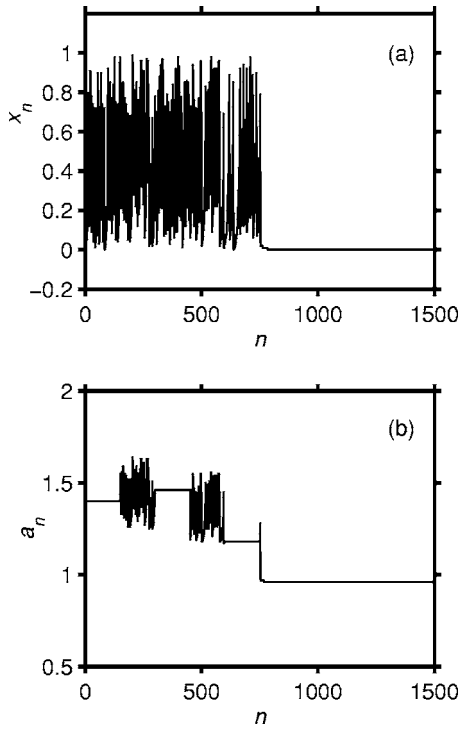

FIG. 1. The value of the dynamical variable x_n versus time step n (a) and the value of the parameter a_n versus time step n (b) for a shift map, where $s=0.4$, $N=150$ and a Haar wavelet filter. a_n is constant if the self-adjustment is off. If the self-adjustment is on and a_n is in the chaotic regime $a_n>1$, the parameter value has an irregular time dependence, but stays within a small range. In this simulation the parameter value a_n, never reaches the boundaries of the parameter range $a_{min}=0$ and $a_{max}=2$.

$$a_{n+1} = a_n + s_n \Delta F_n, \tag{1}$$

where the wavelet filter $\Delta F_n=\Sigma_{j=0}^{M-1} g_j x_{n+1-j}$ has finite support M and zero mean. For Daubechies wavelets of order one with support $M=4$ the wavelet coefficients are $g_0=(1-\sqrt{3})/\sqrt{2}$, $g_1=-(3-\sqrt{3})/\sqrt{2}$, $g_2=(3+\sqrt{3})/\sqrt{2}$, and $g_3=-(1+\sqrt{3})/\sqrt{2}$ [26]. For a Haar wavelet the coefficients are $g_0=-g_1=1$. During the adaption periods the size of the feedback is small and constant, i.e., $0<s_n=s\ll 1$ at the time step $n=iN$, $iN+1,\ldots,(i+1)N-1$, $i=1,3,\ldots$. During the relaxation periods, $n=iN$, $iN+1,\ldots,(i+1)N-1$, $i=0,2,\ldots,I$ there is no feedback, i.e., $s_n=0$. For systems with a bounded parameter range, $a_{min}\leqslant a_n\leqslant a_{max}$, the parameter is set equal to the boundary value if the new value would be outside the parameter range, i.e., $a_{n+1}=a_{max}$ if $a_n+s_n\Delta F_n>a_{max}$ and $a_{n+1}=a_{min}$ if $a_n+s_n\Delta F_n<a_{min}$. Further we assume that the adaptation and relaxation periods are long compared to the support of the filter, i.e., $N\gg M$, and long compared to the relaxation time of the dynamical system x_{jN}, $j=1,2,\ldots$, so that it can reach the vicinity of an attractor before adaptation is turned on or off again. The initial state x_0 is assumed to be random and equally distributed.

Figure 1 shows typical numerical results generated from Eq. (1) for the shift map $f=\mathrm{mod}(a_n x_n+r_n)$, where $-5\times10^{-6}<r_n<5\times10^{-6}$ are random and equally distributed and $0\leqslant a_n\leqslant 2$. The modulo function is defined as $\mathrm{mod}(x)=x-\mathrm{int}(x)$, where $\mathrm{int}(x)$ returns the integer portion of x. If the initial parameter value is in the chaotic regime, i.e., $a_n>1$ the parameter value is changing within a certain range during the adaptation periods. Even though a_n stays within a small range during each adaptation period, these ranges are different at each adaptation period and eventually the parameter value reaches the period regime $a_n<1$ and stays there.

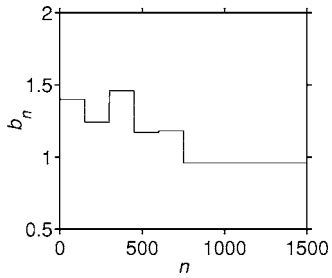

FIG. 2. The value of $b_n=a_n-sF_n$ versus time step n. This plot illustrates that b_n is a conserved quantity except when the self-adjustment is switched on/off.

The *total wavelet filter* is defined as

$$F_n := \sum_{j=0}^{M-1} w_j x_{n-j}, \tag{2}$$

where $w_j=\Sigma_{k=0}^{j} g_k$, $j=0,1,\ldots,M-1$ are the coefficients of the *integrated wavelet*. $w_{M-1}=\Sigma_{k=0}^{M-1} g_k=0$, since we assume that the wavelet has zero mean. Hence $F_{n+1}-F_n=\Delta F_n$ and $F_n=F_{n_0}+\Sigma_{i=n_0}^{n-1}\Delta F_i$ if $n_0\leqslant n$. In contrast to the parameter a_n, the quantity b_n defined as

$$b_n = a_n - s_n F_n, \tag{3}$$

is conserved, i.e.

$$b_{n+1} = b_n \quad \text{if } s_{n+1} = s_n, \tag{4}$$

since $b_{n+1}=a_{n+1}-s_{n+1}F_{n+1}=(a_n+s_nF_{n+1}-s_nF_n)-s_{n+1}F_{n+1}=(a_n-s_nF_n)-(s_{n+1}-s_n)F_{n+1}=a_n-sF_n=b_n$, except when $s_{n+1}\neq s_n$ at the time steps when the adaptation is switched on or off. If a_n reaches the boundary of the parameter range during the adaption period, b_n is not constant. Then $b_n=b_{iN}+\Sigma_{m=iN}^{n-1}(a_{m+1}-a_m-s_m\Delta F_m)$, where s_m is constant. In the following we consider trajectories where a_n does not reach the boundary. Figure 2 shows the time dependence of b_n for the dynamics in Fig. 1.

We can use the conserved quantity to eliminate the dynamical variable a_n from Eq. (1)

$$x_{n+1} = g(x_n, \ldots, x_{n-M+2}, s_n, b_{iN}), \tag{5}$$

where $g(x_n,\ldots,x_{n-M+1},s,b_{iN})=f(x_n,b_{iN}+sF_n)$ and $F_n=F(x_n,\ldots,x_{n-M+2})$. While the conserved quantity is constant during the adaptation periods and the relaxation periods, it may change whenever the adaptation is switched on or off.

From Eqs. (1) and (4) we conclude that the dynamics of b_n, as illustrated in Fig. 2, is governed by the mapping function

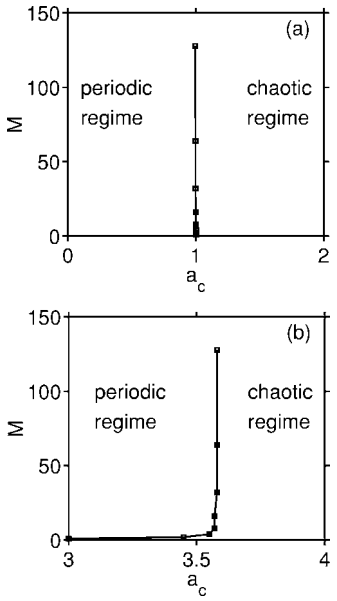

FIG. 3. The edge of chaos a_c as detected by a wavelet filter as a function of length of the support M, for the shift map $x_{n+1}=\mathrm{mod}(a_n x_n+r_n)$ (a) and a logistic map $x_{n+1}=a_n x_n(1-x_n)$ (b). The wavelet coefficients are $g_0=1$, $g_{M-1}=-1$, and $g_i=0$ for $i=1,2,\ldots,M-2$. The threshold is $\Delta F_t=0.002$. The theoretical values are $a_c=3.57$ for the logistic map and $a_c=1$ for the shift map.

$$b_n=\begin{cases} b_{n-1}-(-1)^i s F_{iN} & \text{if } n=iN,\ i\in\mathbb{N} \\ b_{n-1} & \text{else,} \end{cases} \tag{6}$$

where F_{iN} is the value of the filter function at the beginning of an adaptation period, for $i=0,2,\ldots$ and otherwise a value of filter function at the beginning of a relaxation period. Since we assume that the adaption and relaxation periods are long enough for the system to reach its attractor, the range of the values of the filter function F_{iN} at the end of each periods depends only on the value of the conserved quantity b, and the size of the feedback s, if there is only one attractor which covers a finite region of the state space. Hence for $i=0,2,\ldots$ we find $F_{iN}\in[F_{min}(b_{iN},s),F_{max}(b_{iN},s)]$ and otherwise $F_{iN}\in[F_{min}(b_{iN},0),F_{max}(b_{iN},0)]$. Whenever adaptation is switched on or off, the conserved quantity changes by a certain amount which is proportional to s

$$\begin{aligned} b_{iN}+sF_{min}(b_{iN},s)\leqslant b_{(i+1)N}\leqslant b_{iN}+sF_{max}(b_{iN},s) \\ \text{if } i=0,2,\ldots, \\ b_{iN}-sF_{max}(b_{iN},0)\leqslant b_{(i+1)N}\leqslant b_{iN}-sF_{min}(b_{iN},0) \quad \text{else.} \end{aligned} \tag{7}$$

Since b_n is conserved during adaptation periods [see Eq. (6)] and M is constant, a_n stays within a small range of order s

$$b_{iN}+sF_{min}(b_{iN},s)<a_n<b_{iN}+sF_{max}(b_{iN},s), \tag{8}$$

where $iN\leqslant n<(i+1)N$ and $i=1,3,\ldots$ (see Fig. 1).

In the following, we assume that for $s=0$ the parameter a of the map dynamics has an edge of chaos at a_e, i.e., there exists a band of width $\epsilon>0$ about a_e such that when $a_e-\epsilon<a_n<a_e$, there exist *only* periodic attractors with periods $k<k_c$, and when $a_e<a_n<a_e+\epsilon$ the dynamics contain chaotic attractors.

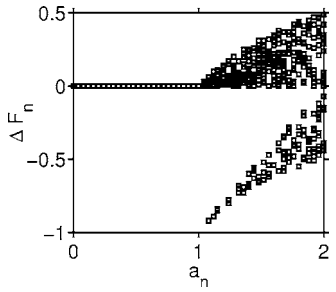

FIG. 4. Typical ΔF_n-values versus the value for the parameter a for a shift map with a Haar wavelet filter. This plot illustrates that $\Delta F_n=0$ if $a_n<a_c$, where $a_c=1$.

Since wavelet filters act as subband filters [26], i.e., low-frequency band filters with cutoff period k_c, they can detect the edge of chaos. The filter output ΔF_n is very small or zero for periodic time series with a recurrence time below k_c, whereas for chaotic time series ΔF_n is irregular. The edge of chaos as detected by the wavelet filter a_c depends on a threshold ΔF_t, i.e., $\max|\Delta F(a_n)|=\Delta F_t$ for $a_n=a_c$ and $\max|\Delta F(a_n)|<\Delta F_t$ for $a_n<a_c$. We determine $\max|\Delta F(a_n)|$ numerically. First we compute a trajectory x_n for a given a_n value and no feedback, $s_n=0$, and then determine the maximum value of the sequence of ΔF_n values, $\max|\Delta F(a_n)|=\max\{\Delta F_n|\Delta F_n:=\Sigma_{j=0}^{M-1}g_j x_{n-j}\}$. Figure 3 shows the edge of chaos a_c for a family of wavelets, including the Haar wavelet, as a function of the length of the support M. The wavelet coefficients of the Haar wavelet are $g_0=1$, $g_{M-1}=-1$, and $g_i=0$ for $i=1,2,\ldots,M-2$. For the shift map and the logistic map wavelets can detect the edge of chaos with reasonable accuracy even if their support is small (see Fig. 3), i.e., $a_c\approx a_e$.

In the following we assume that the limiting value of ΔF is zero, i.e., $\Delta F\approx 0$ for $a_n<a_c$ in a system with no feedback $s=0$. Figure 4 shows the self-adjustment ΔF_n versus a_n for a shift map where $a_c=1$. For a system with feedback we conclude from Eq. (1) that if the parameter value is once below the edge of chaos during a relaxation period, then the self-adjustment is zero from then on, hence for all $n\geqslant iN$

$$\Delta F_n=0 \quad \text{if} \quad a_{iN}<a_c, \tag{9}$$

and if $i\in\{0,2,\ldots\}$. This means that the periodic boundary region is an attractor for the parameter dynamics.

To investigate the statistical properties of the system, we study a large ensemble where the initial parameter values are homogeneously distributed in the interval $I=[a_{min},a_{max}]$, where a_{min} and a_{max} are far away from the edge of chaos, so that the boundary has no impact on the parameter dynamics near the edge of chaos. $P_n(b)$ is probability density of the b_n values at time n, hence $P_0=1/(a_{max}-a_{min})$. Since $a_n=b_n$ during the relaxation periods, the probability density of the a_n values equals the probability density of the b_n values, i.e., the probability density of the a_n values is $P_n(a)$. Next we discuss the change of the b_n values from relaxation period to relax-

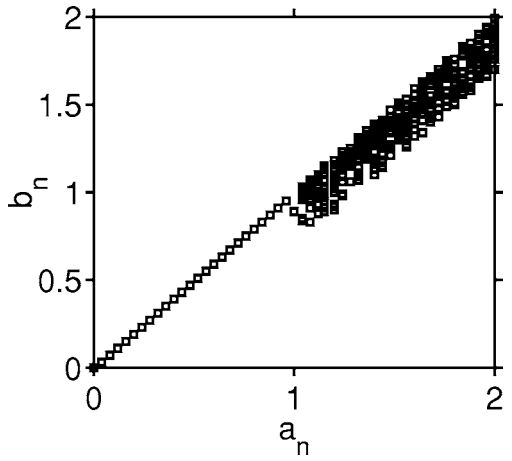

FIG. 5. Typical b values during the adaptation period versus the value for the parameter a during the preceding relaxation period for a shift map with a Haar wavelet filter and $s=0.3$. This plot illustrates that $b_n=a_n$ if $a_n<a_c$, where $a_c=1$.

ation period and how this affects P_n. If the parameter value is below the edge of chaos it is constant even during adaptation periods [see Eq. (9)]. Hence, in the period regime the probability density P_n of the parameter b stays same or increases at the expense of the probability density in the chaotic regime for each b value

$$P_{(i+2)N} \geqslant P_{iN} \quad \text{if } b < a_c \tag{10}$$

for $i \in \{0,2,\ldots\}$. In the following we show that growth of the probability density occurs mostly in the boundary of the periodic regime. Since the b_n changes only by a small amount given by Eq. (7) whenever adaptation is switched on or off, and otherwise b_n is constant, only parameter values in the vicinity of the edge of chaos can reach the periodic regime during one adaptation period. Systems with parameters further away from the edge of chaos can thus reach the periodic regime only after adaptation has been repeatedly switched on and off.

Systems with $b_{iN}>a_c$ during the relaxation period may have a parameter value below a_c during the adaptation period. Figure 5 shows typical b values during the adaptation period values as a function of the a value during the relaxation period for a shift map. Next we consider the case where the b value is in the chaotic regime during a relaxation period.

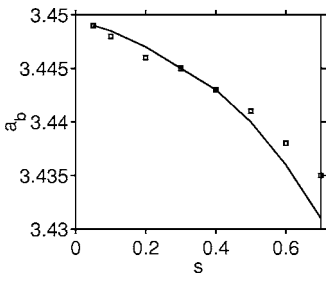

FIG. 6. The lower bound of the periodic boundary regime a_b. The squares indicate numerical values, the continuous lines defined by Eq. (12) for a logistic map $x_{n+1}=a_n x_n(1-x_n)$ with a Haar wavelet filter, where $a_c=3.449$. The probability density increases in the interval $a_b<a<a_c$.

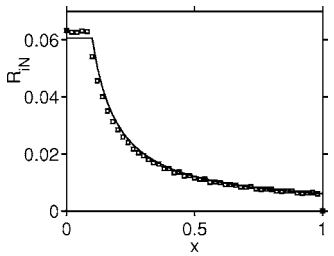

FIG. 7. $R_{x,iN}(x_r)=\rho_{x,iN}(x_r)*\Delta x$, the probability of the x_n values in a bin of size $\Delta x=0.04$ of a self-adjusting shift map with a Haar wavelet filter and $s=0.3$. The squares are a histogram of the numerical values of relative class frequencies of the x-values determined numerically where the sample size is $N=10^6$.

The minimum b value during the next adaptation period is the lowest b value in the chaotic regime minus the maximum change of the b values when the adaptation starts, i.e., $b_{min}=a_c-sF_{max}(a_c,0)$. This assumes that b values which are initially inside the chaotic regime do not have a significantly larger change. Hence the b values which the system can reach from the edge of chaos is lower than the b values that it can reach from inside the chaotic regime, $a_c-sF_{max}(a_c,0)\leqslant b-sF_{max}(b,0)$ for $b>a_c$. This is the case if $F_{max}(b,0)$ does not increase rapidly at the edge of chaos, i.e., $(F_{max}(b,0)-F_{max}(a_c,0))/(b-a_c)\leqslant 1/s$.

We use the same kind of reasoning to estimate the minimum b value during the following relaxation period. The minimum b value during the following relaxation period is $a_b=b_{min}+sF_{min}(b_{min},s)$. This assumes that b values which are initially above b_{min} do not have a significantly smaller change. Hence the b values which the system can reach from b_{min} is lower than the b values that it can reach from b values that are above b_{min}, i.e., $b_{min}+sF_{min}(b_min,s)\leqslant b+sF_{min}(b,s)$ for $b>b_{min}$. This is the case if $F_{min}(b,s)$ does not decrease rapidly at the b_{min}, i.e., $(F_{min}(b,s)-F_{min}(b_{min},s))/(b-b_{min})\geqslant -1/s$.

Next we have to check if $a_b<a_c$. If this is the case then b values that are initially above a_c can end up in the interval $[a_b,a_c]$ within one adaptation/relaxation cycle. Once they are in this interval they are trapped since this interval is in the

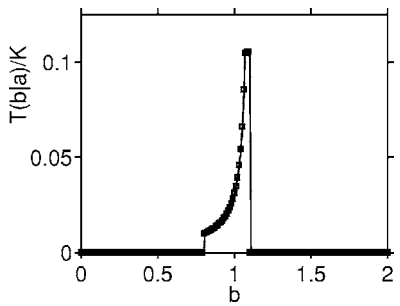

FIG. 8. Shows the conditional transition probability $T(b|a)/K$ of the conserved quantity at the beginning of the adaptation period and the corresponding numerical class frequencies (squares) for $a=1.1$, sample size $N=10^6$, $s=0.3$, and $K=200$ classes.

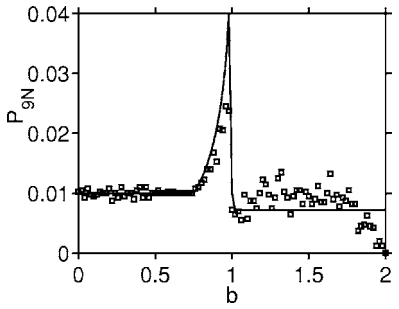

FIG. 9. The numerical values of the relative class frequencies (squares) and the probabilities of the b values $P_{9N}=p_{9N}/K$ of a self-adjusting shift map with a Haar wavelet filter for $s=0.25$, $N=500$, and $K=100$.

periodic regime and their b value does not change from then on. Typically $a_b=a_c-sF_{max}(a_c,0)+sF_{min}(b_{min},s)$ is less than a_c since $F_{min}(b_{min},s)\approx F_{min}(a_c,0)<F_{max}(a_c,0)$.

If $a_b<a_c$ then we conclude from Eq. (7) that the probability density of the b values increases in the periodic boundary region and remains constant in the remainder of the periodic regime

$$P_{(i+2)N}\begin{cases}>P_{iN} & \text{if } a_b\leqslant b\leqslant a_c\\ =P_{iN} & \text{if } b<a_b,\end{cases} \tag{11}$$

for $i\in\{0,2,\ldots\}$, where $a_b=a_c-sF_{max}(a_c,0)+sF_{min}(a_c-sF_{max}(a_c,0),s)$. The periodic boundary region, $a_b\leqslant b\leqslant a_c$ is just below a_c. If we approximate $F_{min}(b_{min},s)\approx F_{min}(b_{min},0)+s*\frac{d}{ds}F_{min}(b_{min},0)+O(s^2)$, we obtain for the lower bound of the periodic boundary region

$$a_b=a_c-s(F_{max}(a_c,0)-F_{min}(b_{min},0))-s^2+O(s^3)\frac{d}{ds}F_{min}(b_{min},0). \tag{12}$$

Figure 6 illustrates the periodic boundary regime for a self-adjusting logistic map dynamics and the parameter range where the class frequencies increase. For the self-adjusting logistic map we find numerically $F_{max}(a_c,0)\approx F_{min}(b_{min},0)$ and $\frac{d}{ds}F_{min}(b_{min},0)\approx 0.036$ for $M=2$. Since the integral of the probability density is equal to one, the increase of the probability density in the periodic boundary region is at the expense of the probability density in the chaotic regime. The migration of the population from the chaotic regime to the periodic boundary region is a concrete model for *adaptation to the edge of chaos*. The population in the chaotic regime evolves toward a narrow regime near the boundary between order and chaos.

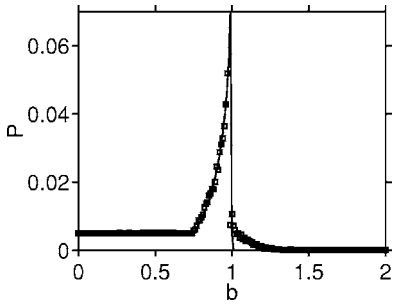

FIG. 10. The numerical values of the limiting relative class frequency (squares) and the limiting probability $P(b)=p(b)/K$ of the b values of a self-adjusting shift map with a Haar wavelet filter, $s=0.25$, $N=500$, and $K=200$.

In the following we compute dynamics of the probability density of the parameter values p_n and the dynamics of the probability density of the x-values ρ_n for a specific example, a self-adjusting shift map $x_{n+1}=\mathrm{mod}(a_n*x_n+r_n)$ with a Haar wavelet filter, where $a_{min}=0$, $a_{max}=2$ and r_n is small band limited white noise, $-10^{-7}<r_n<10^{-7}$. For the self-adjusting shift map, the edge of chaos is $a_c=1$ and $F_{max}(a_c,0)=1$ and $F_{min}(b_{min},0)=0$. Therefore the periodic boundary region is $1-s<b<1$.

If $0\leqslant b_{iN}<1$, the dynamics have a fixed point at $x_n=0$, and the limiting probability density of the x_{iN} values for $s=0$ is $\rho_{iN}=\delta(x)$, where δ is the Kronecker's δ function. For $b_{iN}=1$ the shift map is the identity map and $\rho_{iN}=\delta(x_0)$. If $b_{iN}>1$, the dynamics are chaotic. For small s, i.e., $0\leqslant s\leqslant 0.3$ and b_{iN} values close to unity, i.e., $1<b_{iN}\leqslant 1.5$, the limiting probability density of the x values can be approximated by

$$\rho_{iN}(x)=\begin{cases}\delta(x) & \text{if } a<\\ \dfrac{a_c d}{b_{iN}-a_c} & \text{if } 0\leqslant x<b_{iN}-a_c\\ d/x & \text{if } b_{iN}-a_c\leqslant x\leqslant 1\\ 0 & \text{else,}\end{cases} \tag{13}$$

where $d=1/[1-\ln(b-a_c)]=\alpha+\beta b+O^2(a_c+0.25-b)$, for $a_c=1$ where $\alpha=(2\ln 2-4)/(1+2\ln 2)^2$, and $\beta=4/(1+2\ln 2)^2$. Figure 7 shows a comparison between a histogram of the numerical class frequencies and analytical results in Eq. (13).

Since $b_{(i+1)N}=b_{iN}-sF_{(i+1)N}=b_{iN}-sx_{(i+1)N}$, the conditional probability $T(b|a)$ that the conserved quantity has the value b during an adaptation period, given that it is the value a during the preceding relaxation period, is $T(b|a)=\rho_{(i+1)N}[(a-b)/s]$ for $i=0,2,\ldots$. Hence we replace x by $(a-b)/s$ in Eq. (13) and obtain

$$T(b|a)=\begin{cases}\delta(a-b) & \text{if } a\leqslant a_c\\ \dfrac{d}{s(a-a_c)}, & \text{if } 0\leqslant\dfrac{a-b}{s}\leqslant a-a_c\\ \dfrac{d}{a-b}, & \text{if } a-a_c\leqslant\dfrac{a-b}{s}\leqslant 1\\ 0 & \text{else.}\end{cases} \tag{14}$$

Figure 8 shows the conditional probability $T(b|a)$ and the corresponding class frequencies for $a=1.1$. The probability

of the conserved quantity $p_{(i+1)N}(b)=\int_{a_{min}}^{a_{max}}T(b|a)p_{iN}(a)da$. For $b<a_c$ this integral simplifies to $p_{(i+1)N}(b)=1+\int_{a_c}^{b+s}T(b|a)p_{iN}(a)da$. For the first few adaptation/relaxation cycles we can assume that the probability density in the chaotic regime near the edge of chaos is roughly constant $p(a)=1$ for $a_c<a<a_c+s$. Then $p_{(i+1)N}(b)=1+\int_{a_c}^{b+s}T(b|a)da=1+\int_{a_c}^{b+s}\frac{d}{a-b}da$. We use the approximation for T given in Eq. (14) and evaluate these integrals. We find that for the initial adaptation/relaxation cycles $i=0,2,\ldots,2(a_{max}-b_c)/s$, the probability of the conserved quantity is approximately

$$p_{(i+1)N}(b)=\begin{cases}1 & \text{if } a_{min}\leq b\leq a_c-s\\ \left(\beta(b+s-b_c)+(\beta b+\alpha)\ln\dfrac{s}{a_c-b}\right)\dfrac{i}{2}+1 & \text{if } a_c-s<b<a_c\\ 1 & \text{if } a_c\leq b\leq a_{max}-\dfrac{is}{2}\\ 1-C/s & \text{if } a_{max}-\dfrac{is}{2}\leq b\leq a_{max},\end{cases}\tag{15}$$

where $C=\int_{a_c-s}^{a_c}\left[\beta(b+s-b_c)+(\beta b+\alpha)\ln\frac{s}{a_c-b}\right]db\approx(\beta+\alpha)s+\frac{\beta}{4}s^2$. During the relaxation periods the probabilities for classes in the periodic regime is the same as during the first adaptation period, $P_{a,2N}a_k=P_{b,2N}a_k$ if $a_k<a_c$. Figure 9 shows the class frequencies for the b values and the probabilities computed with Eq. (15).

Next we consider the limiting population after many cycles. Equation (15) indicates that the population in the periodic boundary region is increasing at each adaption/relaxation cycle, until the chaotic regime is depopulated. Therefore we set the probability density in the chaotic regime equal to zero. In addition we normalize i in the expression for the probability density in the periodic boundary region, by a factor which makes the integral of the probability density equal to one, i.e., $\int_0^1 p_{(i+1)N}(b)=1$. With these two steps we obtain from Eq. (15)

$$p(b)=\begin{cases}1 & \text{if } a_{min}\leq b\leq a_c-s\\ \left(\beta(b+s-a_c)+(\beta b+\alpha)\ln\dfrac{s}{a_c-b}\right)\Big/\,C+1 & \text{if } b_c-s<b_k<b_c\\ 0 & \text{if } a_c\leq b\leq a_{max}.\end{cases}\tag{16}$$

Equation (16) models the limiting distribution of the population after many adaptation/relaxation cycles. Figure 10 shows the limiting class frequencies for the b values and the limiting probabilities computed with Eq. (16).

This example illustrates that after many adaptation/relaxation cycles even systems which are initially far away from the edge can migrate into the periodic boundary regime [see Eq. (16) and Fig. 10]. Then the period boundary regime is a global attractor for the parameter dynamics. In contrast, for a single adaptation/relaxation cycle only systems very close to the edge of chaos can migrate into the periodic boundary regime due to the conserved quantity [see Eq. (7)]. During each cycle, adaptation to the edge of chaos is a very local phenomenon. The periodic boundary regime is an attractor for the parameter dynamics, but the basin of attraction is small.

III. CONCLUSION

Many dynamical systems have an edge of chaos in their parameter spaces. On one side of this edge, the dynamics is chaotic for many parameter values, on the other side of the edge it is periodic for all parameter values. Our work shows that discrete-time dynamical systems with wavelet filtered feedback from the dynamical variable to the parameters can be attracted to a narrow parameter range near the edge of chaos, the periodic boundary regime.

We have shown that all self-adjusting map dynamics with wavelet filtered feedback [see Eq. (1)] has a conserved quantity [see Eq. (4)], if the wavelet filer has a finite support and a zero mean. This conserved quantity can be used to eliminate the parameter dynamics from Eq. (1) and to obtain a much simpler mapping function [Eq. (5)]. We used this simpler mapping function to show that the parameter dynamics is bounded during an adaptation/relaxation cycle [see Eqs. (7) and (8)]. Then we showed numerically that subband filters, including wavelets, are typically good chaos detectors, i.e., the filter value is zero or very small for periodic motion, and rather large for chaotic motion. We describe the wavelet's ability to differentiate between periodicity and chaos with the function F_{max} and F_{max} and showed that adaptation to a narrow parameter regime near the edge of chaos occurs [see Eq. (11)], if the wavelet filter is a sufficiently good chaos detector [see Eq. (12)]. Finally we studied one system in detail: adaptation to edge of chaos of shift map with a Haar wavelet filtered feedback. We showed that this theory predicts the dynamics of the probability density [see Eqs. (13)–(16)].

ACKNOWLEDGMENTS

This material is based upon work supported by the National Science Foundation under Contracts Nos. NSF PHY 01-40179, NSF DMS 03-25939 ITR, and NSF DGE 03-38215. M.B. gratefully acknowledges support from the Fannie and John Hertz Foundation, and the National Defense Science and Engineering Program sponsored by the Department of Defense.

[1] S. A. Kauffman, *The Origins of Order: Self-Organization and Selection in Evolution* (Oxford University Press, New York, 1993).
[2] V. V. Alexeev and A. Y. Loskutov, Dokl. Akad. Nauk SSSR **293**, 1346 (1987).
[3] A. Hubler, Helv. Phys. Acta **62**, 343 (1989).
[4] A. Hubler and E. Luscher, Naturwiss. **76**, 67 (1989).
[5] E. A. Jackson and A. Hubler, Physica D **44**, 407 (1990).
[6] J. L. Breeden, F. Dinkelacker, and A. Hubler, Phys. Rev. A **42**, 5827 (1990).
[7] B. B. Plapp and A. W. Hubler, Phys. Rev. Lett. **65**, 2302 (1990).
[8] R. Lima and M. Pettini, Int. J. Bifurcation Chaos Appl. Sci. Eng. **8**, 1675 (1998).
[9] B. R. Andrievskii and A. L. Fradkov, Autom. Remote Control (Engl. Transl.) **64**, 673 (2003).
[10] N. H. Packard, in *Dynamic Patterns in Complex Systems*, edited by J. A. S. Kelso, A. J. Mandell, and M. F. Schlesinger (World Scientific, Singapore, 1988), pp. 293–301.
[11] M. Mitchell, P. T. Hraber, and J. P. Crutchfield, Complex Syst. **7**, 89 (1993).
[12] P. Bak, C. Tang, and K. Wiesenfeld, Phys. Rev. A **38**, 364 (1988).
[13] G. Paladin, M. Serva, and A. Vulpiani, Phys. Rev. Lett. **74**, 66 (1995).
[14] V. Loreto, G. Paladin, and A. Vulpiani, Phys. Rev. E **53**, 2087 (1996).
[15] G. Boffetta, M. Cencini, M. Falcioni, and A. Vulpiani, Phys. Rep. **356**, 367 (2002).
[16] V. P. Zhigulin, M. I. Rabinovich, R. Huerta, and H. D. I. Abarbanel, Phys. Rev. E **67**, 021901 (2003).
[17] D. Pierre and A. Hubler, Physica D **75**, 343 (1994).
[18] C. A. Langton, Physica D **42**, 12 (1990).
[19] A. Adamatzky and O. Holland, Chaos, Solitons Fractals **9**, 1233 (1998).
[20] G. M. Zaslavsky, Phys. Rep. **371**, 461 (2002).
[21] F. Cecconi, D. del Castillo-Negrete, M. Falcioni, and A. Vulpiani, Physica D **180**, 129 (2003).
[22] P. Melby, J. Kaidel, N. Weber, and A. Hubler, Phys. Rev. Lett. **84**, 5991 (2000).
[23] P. Melby, N. Weber, and A. Hubler, Fluct. Noise Lett. **2**, L285 (2002).
[24] L. O. Chua, M. Komuro, and T. Matsumoto IEEE Trans. Circuits Syst. **33**, 1072 (1986).
[25] I. Daubechies, *Ten Lectures on Wavelets*, No. 61 in CBMS-NSF Series in Applied Mathematics (Society for Industrial and Applied Math., Philadelphia, 1992).
[26] *Ripples in Mathematics: the Discrete Wavelet Transform, Wavelet Analysis and Its Applications*, edited by A. Jense and A. la Cour-Harbo (Springer, New York, 2001).
[27] G. Beylkin, R. Coifman, and V. Rokhlin, Commun. Pure Appl. Math. **44**, 141 (1991).
[28] A. H. Tewfik, D. Sinha, and P. Jorgensen, IEEE Trans. Inf. Theory **38**, 747 (1992).
[29] D. F. Walnut, *An Introduction to Wavelet Analysis, Applied and Numerical Harmonic Analysis* (Birkhauser, Boston, 2003).
[30] A. Arneodo, G. Grasseau, and M. Holschneider, Phys. Rev. Lett. **61**, 2281 (1988).
[31] F. Argoul, A. Arneodo, J. Elezgaray, G. Grasseau, and R. Murenzi, Phys. Lett. A **135**, 327 (1988).
[32] F. Argoul, A. Arneodo, J. Elezgaray, G. Grasseau, and R. Murenzi, Phys. Rev. A **41**, 5537 (1990).
[33] F. Argoul, A. Arneodo, G. Grasseau, Y. Gagne, E. J. Hopfinger, and U. Frisch, Nature (London) **338**, 51 (1989).
[34] J. F. Muzy, E. Bacry, and A. Arneodo, Phys. Rev. Lett. **67**, 3515 (1991).
[35] M. Yamada and K. Ohkitani, Prog. Theor. Phys. **86**, 799 (1991).
[36] B. J. Turner and M. Y. LeClerc, J. Atmos. Ocean. Technol. **11**, 205 (1994).
[37] T. Dallard and F. K. Browand, J. Fluid Mech. **247**, 339 (1993).
[38] D. Mackenzie, *Wavelets: Seeing the Forest—and the Trees*, Beyond Discovery (National Academy of Sciences, Washington, 2001).
[39] M. Vergassola and U. Frisch, Physica D **54**, 58 (1991).
[40] S. Qian and J. Weiss, J. Comput. Phys. **106**, 155 (1993).
[41] M. Vergassola and U. Frisch, Physica D **54**, 58 (1991b).